

1-16-2026

## Noninvasive condition monitoring for eccentricity fault detection in large hydro generators

ATENA TAZIKEH LEMESKI


DİDEM TEKGÜN

OZAN KEYSAN

KEMAL LEBLEBİCİOĞLU

MURAT GÖL

Follow this and additional works at: <https://journals.tubitak.gov.tr/elektrik>

 Part of the [Computer Engineering Commons](#), [Computer Sciences Commons](#), and the [Electrical and Computer Engineering Commons](#)

### Recommended Citation

LEMESKI, A. T, TEKGÜN, D, KEYSAN, O, LEBLEBİCİOĞLU, K, & GÖL, M (2026). Noninvasive condition monitoring for eccentricity fault detection in large hydro generators. *Turkish Journal of Electrical Engineering and Computer Sciences* 34 (1): 67-83. <https://doi.org/10.55730/1300-0632.4163>



This work is licensed under a [Creative Commons Attribution 4.0 International License](#).

This Research Article is brought to you for free and open access by TÜBİTAK Academic Journals. It has been accepted for inclusion in Turkish Journal of Electrical Engineering and Computer Sciences by an authorized editor of TÜBİTAK Academic Journals. For more information, please contact [academic.publications@tubitak.gov.tr](mailto:academic.publications@tubitak.gov.tr)

## Noninvasive condition monitoring for eccentricity fault detection in large hydro generators

Atena Tazikeh LEMESKI<sup>1</sup>, Didem TEKGÜN<sup>2,\*</sup>, Ozan KEYSAN<sup>1</sup>,  
Kemal LEBLEBİCİOĞLU<sup>1</sup>, Murat GÖL<sup>1</sup>

<sup>1</sup>Department of Electrical and Electronics Engineering, Middle East Technical University, Ankara, Türkiye

<sup>2</sup>Department of Electrical and Electronics Engineering, Abdullah Gül University, Kayseri, Türkiye

Received: 06.08.2025

Accepted/Published Online: 15.11.2025

Final Version: 16.01.2026

**Abstract:** Eccentricity faults in electric machines remain a critical concern, as they generate uneven magnetic forces that increase vibration and noise, ultimately raising the risk of premature motor failure. This study proposes a method for the early detection of dynamic eccentricity (DE) faults in hydropower plants through an advanced optimization-based parameter identification technique integrated with finite element analysis (FEA). Finite element modeling (FEM) is first used to analyze an existing salient-pole synchronous generator (SPSG) from a hydroelectric power plant in Türkiye. The effects of DE faults on the SPSG's magnetic equivalent circuit parameters are then examined under various fault severities. A comprehensive hydropower plant model—including the synchronous generator, governor, and excitation system—is developed in MATLAB/Simulink, with all input parameters obtained from real plant data and equivalent circuit variations extracted from FEA. After completing the modeling stage, including fault scenarios, MATLAB and Simulink are employed together to estimate key magnetic equivalent circuit parameters using a modified particle swarm optimization (MPSO) algorithm, achieving highly accurate parameter estimation. Since the hydropower system allows measurement of the three-phase output currents, parameter estimation is performed based on current variations under different fault conditions. The simulation results verify the method's ability to detect faults with high accuracy; thus, this integrated and noninvasive approach provides a robust framework for ensuring the operational reliability and longevity of large hydro generators.

**Key words:** Salient pole synchronous generator (SPSG), parameter identification, condition monitoring, fault detection, finite element modeling (FEM)

### 1. Introduction

Synchronous generators (SGs) with salient poles are the preferred choice for hydroelectric power plants due to the low rotational speed requirements of the prime mover [1]. The detection and diagnosis of faults in such large electrical machines are crucial to maintaining the reliability and efficiency of power generation systems [2]. Faults in SGs can occur in various components, including bearings, stator, rotor field windings, damper windings, and the air gap, and are generally classified as either (i) electrical or (ii) mechanical. Among these, mechanical faults—particularly air-gap eccentricity—account for more than 50%.

\*Correspondence: didem.tekgun@agu.edu.tr

Dynamic eccentricity (DE) faults are of particular concern due to their potential to cause severe damage and prolonged downtime [3, 4]. DE occurs when the rotor's rotational center deviates from its geometric center, resulting in an irregular air gap between the rotor and stator [5, 6]. This condition leads to abnormal vibrations, increased losses, and accelerated wear of machine components. Therefore, early detection of DE faults is critical to prevent catastrophic failures [7]. Recent research on eccentricity fault detection has explored a variety of diagnostic techniques, including current signature analysis [2, 8, 9], stator terminal voltage monitoring [5, 10–12], and magnetic field analysis [13–16]. Eccentricity fault detection based on current harmonic analysis has been extensively investigated [17, 18]; however, the resulting harmonics are highly dependent on the specific geometry and structure of the SG, which may cause overlap with power network harmonics [19]. Reference [20] proposes a real-time method for detecting eccentricity faults in permanent magnet machines by estimating the fault using voltage measurements from search coils positioned within the air gap. Similarly, [21] provides an in-depth analysis of the magnetic characteristics of SGs under both static eccentricity (SE) and DE conditions, focusing on the external electromagnetic field. In [22], SE and DE faults are examined through analysis of the stray magnetic field using two search coils mounted on the backside of the stator yoke in conjunction with advanced signal processing techniques. A comprehensive review of air-gap eccentricity detection methods is presented in [23], where finite element modeling (FEM), analytical modeling, and equivalent circuit parameter approaches are compared in terms of their sensitivity and accuracy for eccentricity detection.

Although the aforementioned methods provide valuable insights into fault detection, each has limitations that reduce their effectiveness for early-stage detection or under varying operating conditions. Stator current analysis is susceptible to false detections and is inapplicable during open-circuit operation. Voltage monitoring faces challenges in detecting minor faults and is influenced by nonlinear loads, while air-gap and stray magnetic field monitoring, despite their sensitivity, require complex signal processing and precise sensor placement. External flux monitoring also demands multiple search coils and measurement instruments to capture subtle changes under faulty conditions. Moreover, these techniques often require extensive data acquisition and analysis, making them less suitable for real-time fault detection in practical operating environments. While FEM provides highly accurate offline analysis, it is limited in real-time fault detection due to its computational complexity and the need for detailed modeling. Although real-time monitoring is not essential for all fault types, it is crucial for detecting early-stage DE faults before they develop into severe mechanical or electromagnetic damage. Conventional offline approaches, by contrast, typically identify DE faults only after they have progressed to advanced stages.

This study presents a noninvasive and highly efficient approach for the early detection of eccentricity faults in a large salient-pole synchronous generator (SPSG) operating within a hydroelectric plant. Finite element analysis (FEA) is utilized to model different severities of DE, thereby creating realistic fault scenarios. A detailed model of the hydropower plant system—comprising the synchronous generator, governor, and excitation system—is developed in MATLAB/Simulink using real operational data from an actual facility. Variations in the SPSG's equivalent circuit parameters, particularly those associated with the magnetic circuit, are extracted from the FEA simulations. The simulation results indicate that key electrical parameters, such as the d-axis synchronous and transient reactances, exhibit significant variations under eccentricity fault conditions. Although minor deviations in these parameters may arise from other influences, the distinct effects of DE make them reliable indicators for fault diagnosis. To achieve high-accuracy parameter estimation, the modified particle swarm optimization (MPSO) algorithm is employed due to its robustness, rapid convergence, and strong capability in managing nonlinear parameter interactions within the generator model [24, 25]. The

estimation process utilizes three-phase output current measurements, which are readily available from the existing plant infrastructure, and evaluates their variations under different fault scenarios. While previous studies have applied FEA for fault analysis or used parameter estimation techniques independently, few have integrated these two approaches specifically for eccentricity fault detection in synchronous generators [26, 27]. Furthermore, the proposed method offers a notable improvement over conventional techniques by significantly reducing the required measurement time, thereby enabling faster and more reliable fault detection.

Furthermore, previous research on eccentricity fault detection has largely depended on analytical modeling, vibration and current signal analysis, or data-driven estimation techniques. Although these methods provide valuable diagnostic insights, they often necessitate additional sensors and demonstrate reduced accuracy under noisy or transient operating conditions. These limitations highlight the need for, and thus motivate, the development of the proposed FEM–MPSO-based framework. Here, ANSYS/ MotorCAD is employed to extract key equivalent circuit parameters, namely the direct-axis synchronous reactance ( $X_d$ ), direct-axis transient reactance ( $X'_d$ ), quadrature-axis reactance ( $X_q$ ), quadrature-axis transient reactance ( $X'_q$ ), and leakage reactance ( $X_l$ ), for the analysis of DE fault scenarios. As the severity of eccentricity increases, changes in magnetic saturation lead to a reduction in the corresponding reactance values. Among these parameters,  $X_d$  and  $X'_d$  exhibit the most significant changes under faulty conditions. Building on this observation, the proposed parameter identification strategy focuses on tracking these specific reactances to enable early and accurate detection of DE faults, thereby enhancing both the reliability and effectiveness of condition monitoring in SGs. The main contributions of this study are:

- A noninvasive and practical fault identification approach that relies solely on stator current measurements, thereby eliminating the need for additional sensors or intrusive testing procedures.
- Integration of FEM with the MPSO algorithm, enabling accurate parameter estimation and fault detection even when physical fault experiments are not feasible.
- A validated simulation framework capable of replicating the behavior of faulty synchronous generators, providing a reliable and cost-effective alternative to hazardous real-machine fault testing.
- Demonstration of practical applicability for real hydro generator monitoring systems, showing that the proposed method can be seamlessly implemented within existing plant instrumentation for continuous condition assessment.

The structure of the paper is organized as follows: Section 2 presents the FEM-based modeling of the system. Section 3 details the implementation of the proposed method, while Section 4 evaluates the simulation results to validate the effectiveness of the approach. Section 5 summarizes the key findings, and Section 6 outlines potential directions for future research.

## 2. Finite element model

In this section, FEM analysis is carried out using ANSYS/ MotorCAD for both healthy and faulty conditions of the SPSG.

### 2.1. SPSG modeling

This section presents the development of a detailed FEM model to investigate the electromagnetic behavior of the SPSG under various operating conditions, including both healthy and faulty states. The analyzed

machine represents a hydropower generator rated at 187.5 MVA, with 26 poles and 222 stator slots. A two-dimensional (2D) electromagnetic model was developed in ANSYS/MotorCAD, as illustrated in Figure 1, and the main specifications are listed in Table 1. While a 2D transient magnetic model is used in this study to analyze the SPSG, it is acknowledged that salient-pole hydro-turbine generators inherently exhibit 3D effects, such as end-region leakage flux, pole-shoe fringing, and axial saturation variations. These effects may locally influence magnetic flux distribution and harmonic content, leading to slight underestimations of local saturation levels in 2D simulations. However, the 2D approach remains a well-established and computationally efficient method for comparative fault studies, as it accurately captures the dominant radial and tangential field components responsible for electromagnetic torque and flux-linkage variations. Therefore, although 3D modeling could provide additional local field detail, the adopted 2D approach sufficiently represents the machine's electromagnetic behavior for identifying and comparing the sensitivity of parameters to different fault types. Here, the primary objective is to assess how different levels of DE influence key performance parameters. DE is a common mechanical fault that occurs when the rotor's center of rotation deviates from its geometric axis while continuing to rotate around the stator axis. Figure 2a and Figure 2b illustrate the healthy and DE fault conditions, respectively. This displacement leads to a nonuniform air gap and causes time-varying magnetic field distortions. The FEM model is developed using a 2D transient magnetic solver, in which the complete geometry of the machine is represented to accurately capture the air-gap variations and the resulting magnetic field distortions caused by the DE fault. The stator and rotor geometries are created, M800-50A laminated steel is assigned to both the stator and rotor cores, while pure copper is used for the stator windings, consistent with the materials employed in the actual hydropower generator. The mesh density was locally refined in critical regions, particularly within the air gap and slot openings, to ensure accurate resolution of magnetic field gradients caused by eccentricity. The boundary conditions were defined using magnetic vector potentials by 100 percent. After establishing the model, the healthy generator is first simulated under rated full-load conditions to obtain the baseline performance metrics. Subsequently, DE faults are introduced by displacing the rotor center from the stator axis by 5%, 10%, 20%, 30%, and 40% of the air-gap length to examine their effects on the electromagnetic field distribution. For each operating condition, transient magnetic simulations are performed for multiple electrical cycles until a steady state is achieved. A time step of 0.2 ms is selected to provide adequate temporal resolution for capturing flux-density variations and changes in the equivalent circuit parameters accordingly.

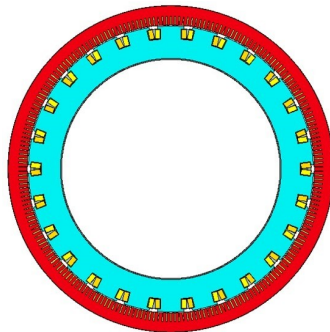


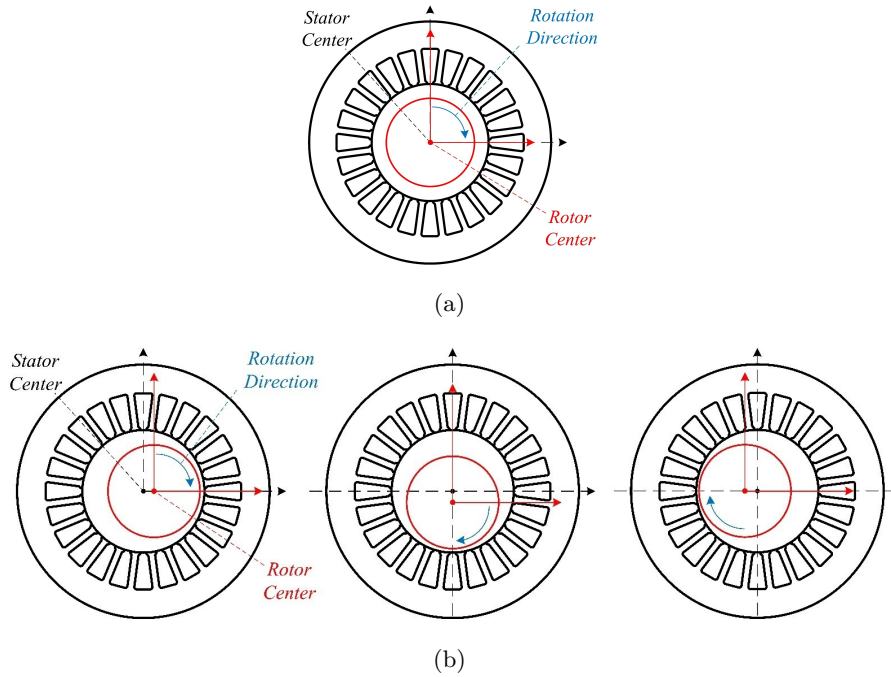
**Figure 1.** Full model cross-section of the SPSG.

Finally, the SPSG was also analyzed under various severities of rotor field winding short-circuit (RFWSC) faults to compare the sensitivity of parameters previously identified under DE conditions. The results confirmed

**Table 1.** Nameplate data of hydropower plant SPSG

Quantity	Value	Unit	Quantity	Value	Unit
Rated Power	187500	kVA	Outer Diameter (Stator)	7380	mm
Power Factor	0.9	-	Inner Diameter (Stator)	6500	mm
Stator Voltage	15.5	kV	Rotor Diameter	6454	mm
Stator Current	6984	A	Airgap Length	23	mm
Exc. Current (Resistive Load)	694.39	A	Stack Length	2170	mm
Frequency	50	Hz	Total Slot Count	222	-
Sync Speed	230.76	RPM	Pole Count	26	-
Slot Depth	198.7	mm	Meshing Size (air gap)	0.3	mm
Slot Opening	24.2	mm	Simulation Type	Transient 2D	-
Tooth Tip Angle	30	Degree	Time Step	0.2	ms

that parameters most affected by DE remain largely unaffected by RFWSC faults, verifying that their variations are primarily associated with mechanical eccentricity rather than electrical disturbances. The parameters most sensitive to DE were subsequently employed in the parameter identification stage using the MPSO algorithm.

**Figure 2.** Motor rotation under; (a) Healthy, (b) DE conditions.

## 2.2. Simulation results

This section presents the analysis of air-gap displacement under varying severities of DE. The developed model is utilized to simulate and evaluate the machine's electromagnetic behavior across five distinct DE levels; 5% (1.2 mm), 10% (2.5 mm), 20% (5 mm), 30% (7.5 mm), and 40% (9.5 mm), all applied at a 45-degree angular position. According to the analysis, Figure 3 illustrates the magnetic flux density distribution of the SPSG under both normal operating conditions and a 40% DE fault. In the healthy state, shown in Figure 3a, the magnetic flux is uniformly distributed across the stator and rotor cores. In contrast, Figure 3b, representing the most severe DE condition, reveals a substantial increase in magnetic flux density on the upper side of the machine due to the reduced air gap, while a corresponding decrease is observed on the lower side where the air gap is enlarged.

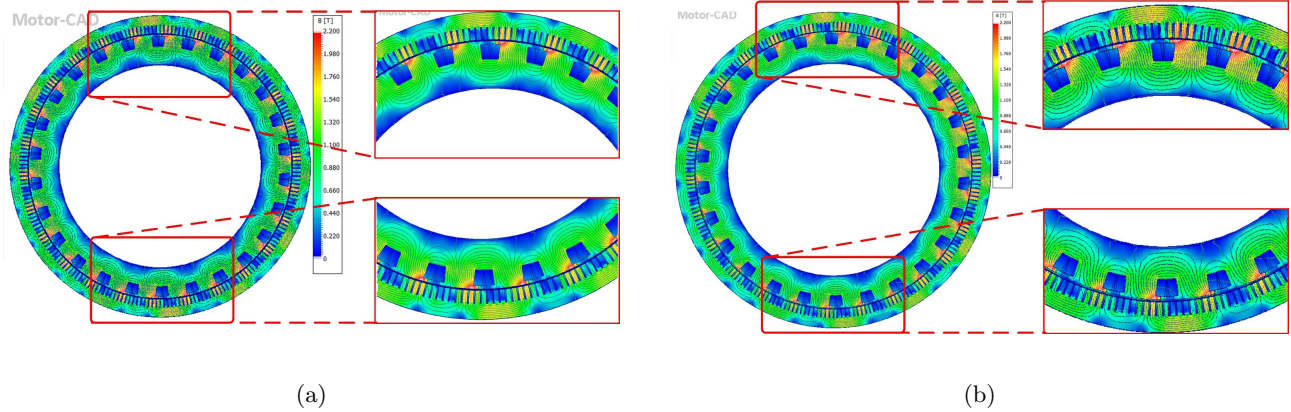


**Figure 3.** The magnetic flux density of SPSG under a) healthy operation and b) 40% of DE faulty operation.

MotorCAD enables the extraction of changes in the equivalent circuit parameters ( $X_d$ ,  $X'_d$ ,  $X_q$ ,  $X'_q$ ), which are subsequently incorporated into the MATLAB/Simulink model of the synchronous generator. The critical extracted parameter results are provided in Table 2.

**Table 2.** Data variation of SPSG parameters under different severity of DE in p.u.

SPSG Parameter	Healthy	5% (1.2mm)	10% (2.5mm)	20% (5mm)	30% (7.5mm)	40% (9.5mm)
$X_d$	1.185	0.987	0.984	0.971	0.950	0.930
$X'_d$	0.680	0.645	0.640	0.638	0.633	0.628
$X_q$	0.794	0.782	0.769	0.767	0.764	0.760
$X'_q$	0.800	0.782	0.769	0.767	0.764	0.760
$X_l$	0.160	0.160	0.160	0.160	0.160	0.160

The results reveal that the parameters most influenced by variations in the air gap are  $X_d$  and the  $X'_d$ , while changes in the  $X_q$  and  $X'_q$  are negligible. Consequently, continuous monitoring of  $X_d$  and  $X'_d$  provides an effective means for detecting air-gap eccentricity. Under DE conditions, a minimum deviation of 16.6% (corresponding to a 1.2 mm fault) and a maximum deviation of 21.2% (corresponding to a 9.5 mm fault) are observed in  $X_d$ . A similar trend is found for  $X'_d$ , though the deviations are slightly smaller, as detailed in Table 2. Additionally, the leakage reactance ( $X_l$ ) is found to be unaffected by eccentricity faults at any severity level, indicating that leakage effects are not significant in such cases.

In addition to mechanical faults, electrical faults are also prevalent in large-scale hydropower SPSGs. Among these, the rotor field winding short-circuit (RFWSC) fault is one of the most common and can occur at different severity levels. To assess its impact, additional analyses are performed in this study, showing that, unlike DE faults, RFWSC faults have a negligible effect on the equivalent circuit parameters of the SPSG. These results confirm that  $X_d$  and  $X'_d$ , which are sensitive to DE faults, remain largely unaffected by electrical faults and can therefore serve as reliable indicators for detecting air-gap eccentricity. Here, A per-unit (p.u.) system is adopted to normalize the parameters of the hydro generator and ensure direct comparability between simulation environments. In this study, the base values are selected according to the generator's rated nameplate data,

consistent with standard industrial practice. The base apparent power ( $S_{base}$ ) corresponds to the generator's rated power, and the base voltage ( $V_{base}$ ) to the rated line-to-line stator voltage. The base reactances ( $X_{base}$ ) are calculated accordingly.

The DE fault is analyzed using ANSYS/ MotorCAD, since this environment allows the eccentricity level to be easily defined by geometric displacement of the rotor center and provides steady-state magnetic equivalent-circuit parameters under various operating conditions. However, the RFWSCF cannot be modeled in MotorCAD due to its simplified electromagnetic representation. Therefore, ANSYS/ Maxwell is employed for RFWSCF simulations, as it enables detailed FEM of short-circuited turns and allows the extraction of steady-state  $X_d$  and  $X_q$ . Although two different ANSYS environments are employed, MotorCAD for DE analysis and Maxwell 2D for RFWSCF simulations, consistency is carefully maintained across both models. The material B-H curves, mesh resolutions, and boundary conditions are aligned to ensure comparable simulation conditions. The air-gap mesh density and refinement levels are also kept consistent, particularly in the critical regions where magnetic field variations are most pronounced. Since both MotorCAD and Maxwell are ANSYS products and use the same electromagnetic material databases and solver algorithms, it is possible to achieve nearly identical magnetic characteristics and field distributions across the two environments. Therefore, the cross-tool consistency ensures that the observed parameter variations are attributable to the fault types themselves rather than modeling discrepancies. Table 3 summarizes the steady-state values of  $X_d$  and  $X_q$  for various levels of RFWSC. Since  $X_d$  exhibits the most significant response to DE faults, it is the primary focus of comparison. Although the variation in  $X_d$  and  $X_q$  4% and 20% RFWSCF appears minor, this difference is within the numerical uncertainty range of the finite element analysis. A convergence study is therefore conducted to ensure the reliability of the results. The mesh size in the air-gap region is progressively refined from 0.3 mm to 0.1 mm in the airgap, and the time-step is reduced to verify the stability of the computed reactances. The resulting variation in both  $X_d$  and  $X_q$  values remain below  $\pm 0.0004$  p.u., confirming that the previously reported differences are indeed within acceptable numerical tolerance. As expected, the results indicate that neither  $X_d$  nor  $X_q$  is significantly affected by RFWSC faults. This outcome can be attributed to the minimal impact of RFWSC on saliency torque, which is directly related to the  $X_d/X_q$  ratio. Nevertheless, minor variations may still occur due to slight changes in the number of turns ( $N$ ) or phase current associated with the RFWSC fault.

**Table 3.** Data variation for healthy and several degrees of RFWSC faults in p.u.

Parameter	Healthy	4% RFWSC	10% RFWSC	20% RFWSC
$X_d$	1.185	1.185	1.185	1.184
$X_q$	0.794	0.7940	0.7943	0.7946

Based on the results obtained for both DE and RFWSC faults, it is evident that generator reactance exhibits a distinct trend in response to mechanical faults, such as DE, as opposed to electrical faults. Specifically,  $X_d$  decreases with increasing severity of DE, indicating that significant variations in  $X_d$  are directly linked to mechanical fault conditions. As a result, the parameters  $X_d$  and  $X'_d$ , which show sensitivity to DE, are extracted from the FEM analysis and used as inputs to the MPSO algorithm for real-time fault detection.

### 3. The proposed method

#### 3.1. Parameter identification in salient pole synchronous generators (SPSGs)

The primary objective of this research is to develop a reliable condition monitoring framework capable of accurately estimating the dynamic parameters of SPSGs. Implementing real faults or intentionally altering

machine parameters in long-operating power plants is impractical and potentially hazardous. To overcome this limitation, the proposed method adopts a simulation-based strategy that employs two representations of the same generator: one serving as the reference model and the other as the unknown system for parameter identification. Rather than relying on real current measurements, the first simulated generator acts as a virtual representation of the physical machine, modeled under both healthy and faulty operating conditions. In the healthy scenario, the generator operates with nominal parameters, ensuring stable and ideal electrical characteristics. In contrast, the faulty case introduces deviations in parameters such as direct-axis synchronous reactance and transient reactance to emulate the effects of DE faults. The second simulation is performed on the same generator, but its parameters are considered unknown. The central concept of the proposed method is to estimate these unknown parameters using the three-phase current obtained from the first simulation. Through an optimization-based approach employing the MPSO algorithm, the parameter estimation process iteratively minimizes the difference between the simulated output and the reference current, thereby achieving accurate identification of the generator's key parameters.

### 3.2. Objective function

The objective function for parameter identification minimizes the sum of squared differences between measured and modeled three-phase currents over a defined period. This function is expressed as follows.

$$\text{Minimize } J = \sum_{n=1}^N \left[ (I_{\text{meas},n}^A - I_{\text{sim},n}^A)^2 + (I_{\text{meas},n}^B - I_{\text{sim},n}^B)^2 + (I_{\text{meas},n}^C - I_{\text{sim},n}^C)^2 \right] \quad (1)$$

where  $I_{\text{meas},n}^{A,B,C}$  are the measured phase currents at time  $n$ ,  $I_{\text{sim},n}^{A,B,C}$  are the corresponding simulated currents from our model, and  $N$  represents the total number of time steps.

The goal of the optimization is to find the set of parameters that minimize this objective function, thereby ensuring the best fit between the measured data and the machine's model. The proposed methodology for fault detection is outlined in Figure. 4, illustrating the sequential steps involved in parameter estimation and fault identification.

### 3.3. Optimization using modified particle swarm optimization (MPSO)

To effectively address the parameter identification problem, the MPSO algorithm is employed. The selection of MPSO is motivated by its superior convergence speed, robustness, and enhanced ability to avoid local minima compared with conventional optimization techniques. In the proposed MPSO approach, the inertia weight is linearly decreased over successive iterations to achieve an optimal balance between exploration and exploitation. The particle velocity is constrained within  $\pm 20\%$  of the parameter range to prevent divergence, while velocity clamping and adaptive inertia mechanisms ensure stable convergence even in the presence of noise. The algorithm's update process follows the standard Particle Swarm Optimization equations for position and velocity updates, and its implementation is carried out in MATLAB.

In MPSO, each particle represents a possible solution, which is a set of estimated parameters for the machine. These particles move through the solution space guided by their own experience and that of other particles; they search for the global minimum of the objective function.

The MPSO algorithm operates according to the following equations, which update the velocity and position of each particle  $i$  at iteration  $k$ :

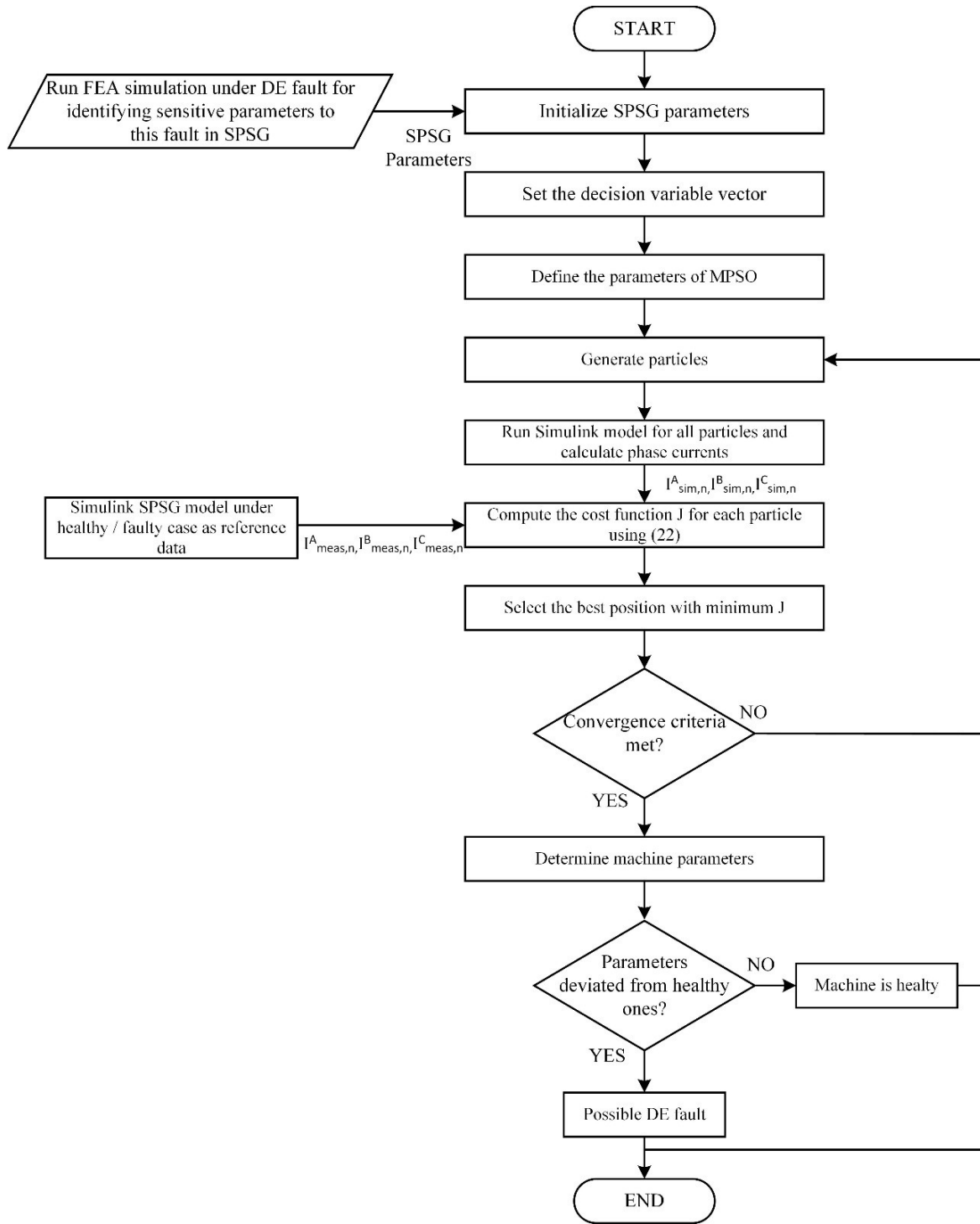


Figure 4. Proposed method.

$$v_i(k+1) = w \cdot v_i(k) + c_1 \cdot r_1 \cdot (p_i - x_i(k)) + c_2 \cdot r_2 \cdot (g - x_i(k)) \quad (2)$$

$$x_i(k+1) = x_i(k) + v_i(k+1) \quad (3)$$

where  $v_i(k)$  is the velocity of particle  $i$  at iteration  $k$ ,  $x_i(k)$  denotes its position,  $p_i$  is the personal best position, and  $g$  represents the global best. The inertia weight is  $w$ , the cognitive and social acceleration coefficients are  $c_1$  and  $c_2$ , and  $r_1, r_2 \in [0, 1]$  are random values.

MPSO adapts over iterations by adjusting the particle velocities and positions, driving the particles toward the optimal parameter set that minimizes the objective function.

### 3.4. Algorithm settings and reproducibility

The MPSO-based parameter identification was implemented in MATLAB with the following parameters: inertia weight  $w = 0.7$ , acceleration coefficients  $c_1 = c_2 = 1.5$ , population size of 10, and a maximum of 50 iterations. To verify robustness, the identification process was repeated under several configurations ( $10 \times 50$ ,  $20 \times 50$ , and  $10 \times 100$ ). The results showed negligible variation in the identified parameters, confirming that the adopted population and iteration settings provide a cost-effective balance between accuracy and computation time.

## 4. Analysis and results

This section evaluates the proposed method's performance through the use of a power plant model. This model offers a streamlined description of the interaction between the synchronous generator, the governor, and the excitation system within the simulation environment. The modeling and simulation aim to confirm the effectiveness of the proposed fault detection approach under realistic operating conditions. The modeled SPSG has a rating of 187.75 MVA, a nominal voltage of 15.5 kV, and operates at 50 Hz with a DC exciter and hydraulic turbine governor. The excitation system is modeled in simulink using a DC exciter, as described in [28]. The primary elements of the excitation system block consist of the voltage regulator and the exciter. The hydraulic turbine and governor block, meanwhile, includes a nonlinear hydraulic turbine model, a PID-driven governor system, and a servomotor.[29]. A case study has been conducted using a simulated real generator to replicate actual operating conditions. The three-phase stator currents were recorded at the generator terminals during startup, capturing data for the first six seconds of operation with a sampling rate of 100 samples per second. This duration was chosen based on the generator's transient response, as it provides sufficient data for identifying variations in key parameters relevant to DE detection. Tests with different data window lengths (1–12 s) showed that the estimation error stabilizes beyond 6 s; therefore, a 6 s window was selected as the optimal balance between precision and computational efficiency. The collected current signals serve as input for the proposed parameter identification method, ensuring that the analysis is based on a high-fidelity simulation that closely mimics the behavior of a real generator under operating conditions. Gaussian noise was added independently to each phase current with a standard deviation of 500 A. Given the start-up currents of 10 kA, this corresponds to an effective signal-to-noise ratio (SNR) of about 25 dB, ensuring realistic robustness testing of the identification method. The simulation has been carried out using MATLAB/ Simulink. The parameters  $X_d$ ,  $X'_d$  are identified as the parameters most affected by the applied DE fault. Consequently, these parameters are employed in the demonstration experiments throughout the remainder of the chapter. Multiple variables have been selected in parameter identification for a more realistic approach, and to see the impact of the healthy parameters on this work. So, for this reason  $H$  and  $X_q$  in addition to  $X_d$  and  $X'_d$  for parameters identification have been considered and all these parameters will be estimated simultaneously. Although all the dynamic parameters are identifiable in this method simultaneously, these parameters have been selected to avoid computational burden and reduce the time of optimization. For a demonstration that we can track the variation, the estimation of these parameters under different percent of variation in the parameters is performed

and has been shown via four different scenarios which are presented below. The parameters of the MPSO algorithm used for parameter identification are crucial for its performance. The key parameters consist of the population size and the maximum iteration count. For the algorithm, parameter boundaries were set as  $[0 \ 0 \ 0 \ 0]$  (lower bound) and  $[4 \ 2 \ 3 \ 12]$  (upper bound) which correspond respectively to  $X_d$ ,  $X'_d$ ,  $X_q$ , and  $H$  (all in per-unit). These limits were selected to reflect physically realistic ranges for synchronous machines while ensuring numerical stability of the identification process...

#### 4.1. Scenario 1: Healthy generator operation

In this scenario, the generator operates under ideal healthy conditions without DE fault or parameter variations. The selected parameters for tracking in the parameter identification process include  $H$ ,  $X_d$ ,  $X_q$ , and  $X'_d$ , which are simultaneously included in the decision variable vector of the MPSO algorithm. To generate the measurements, we used simulation-based data derived from nominal generator operating conditions. This allowed for the collection of a dataset against which the MPSO algorithm could be tested. The results presented in Table 4 demonstrate a low identification error, consistently below 1%. The measurement errors for each trial were calculated by comparing the estimated values with the nominal and actual values. These small deviations confirm the accuracy of the identification process. By maintaining a steady error margin across all parameters, the method establishes a reliable baseline for future fault detection efforts. This solid baseline ensures that any deviations observed in faulted conditions can be confidently attributed to the presence of a fault rather than inconsistencies in the parameter identification process.

**Table 4.** The results statement of scenario 1.

Parameter (p.u.)	Estimated Value (MPSO)	Nominal Value	Error (%)
$H$	3.21	3.2	0.3
$X_d$	1.19	1.18	0.8
$X_q$	0.797	0.8	0.3
$X'_d$	0.685	0.68	0.73

#### 4.2. Scenario 2: Parameter identification under eccentricity fault

In this scenario, an eccentricity fault of 10% was introduced and two separate identification methods were performed to detect the fault using the MPSO algorithm.

##### 4.2.1. Case 1: Identification of $H$ , $X_d$ , $X'_d$ , $X_q$ .

Initially, four parameters were selected for identification:  $H$ ,  $X_d$ ,  $X'_d$ , and  $X_q$ . The rationale behind this approach was to include as many parameters as possible in the identification process to observe how the system behaves under faulty conditions and to identify any deviations in parameters sensitive to eccentricity.

The results indicate that there are significant differences between the nominal and estimated values of the parameters  $X_d$  and  $X'_d$ , which showed substantial changes in the presence of eccentricity fault. This provides an early warning alert, as the decrease in  $X_d$  by 17% and in  $X'_d$  by 6% clearly indicates the presence of the fault. However, because of limited measurements and low redundancy, the overall error in the estimation remains relatively high. The estimated values for the other parameters,  $H$  and  $X_q$ , did not show significant variations,

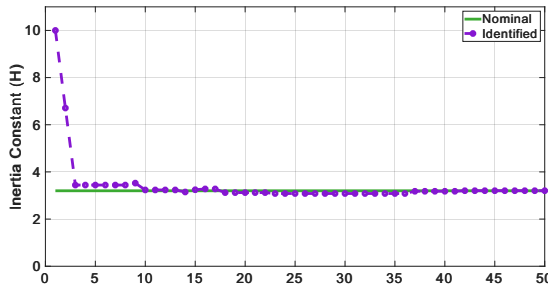
suggesting that these parameters were less affected by the eccentricity fault, and therefore, the estimation bias is limited.

Table 5 summarizes the results for the identification of four parameters. Figure 5 illustrates the identification of all four parameters. Specifically, Figure 5a shows the estimation of  $H$ , Figure 5b presents  $X_d$ , Figure 5c shows  $X'_d$ , and Figure 5d corresponds to  $X_q$ .

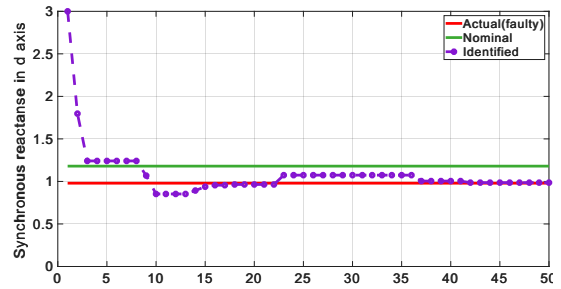
Additionally, the convergence curve for the MPSO algorithm used in the four-parameter identification process is shown in Figure 6. This demonstrates the reduction in the best cost function over 50 iterations.

**Table 5.** The results statement of scenario 2, case 1.

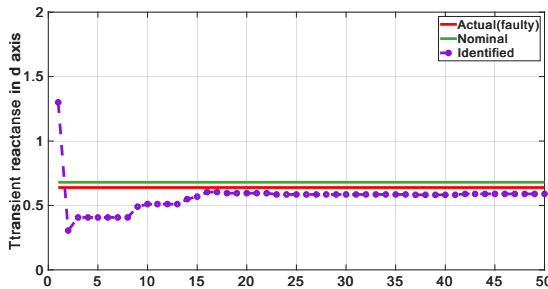
Parameter (p.u.)	Estimated Value (MPSO)	Nominal Value	Actual (Faulty) value	Error (%)
$X_d$	0.9860	1.18	0.984	0.2
$X'_d$	0.5896	0.68	0.64	7.87
$H$	3.2031	3.2	-	0.09
$X_q$	0.8177	0.8	-	2.2



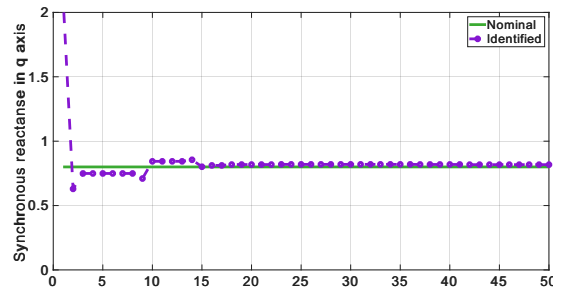
(a) Identification of  $H$



(b) Identification of  $X_d$



(c) Identification of  $X'_d$



(d) Identification of  $X_q$

**Figure 5.** Parameter identification ( $H$ ,  $X_d$ ,  $X'_d$ ,  $X_q$ ) for scenario 2, case 1.

#### 4.2.2. Case 2: Identification of $X_d$ , , $X'_d$

In the second part of the scenario, a more focused identification was carried out by limiting the identification process to the two most sensitive parameters:  $X_d$  and  $X'_d$ . This approach assumes that the rest of the system is healthy and that only the parameters affected by the eccentricity fault need to be identified. Figure. 7a and Figure. 7b display the identification of  $X_d$  and  $X'_d$  respectively. The results showed a significant improvement in estimation accuracy, with the errors for both  $X_d$  and  $X'_d$  decreasing compared to the previous identification

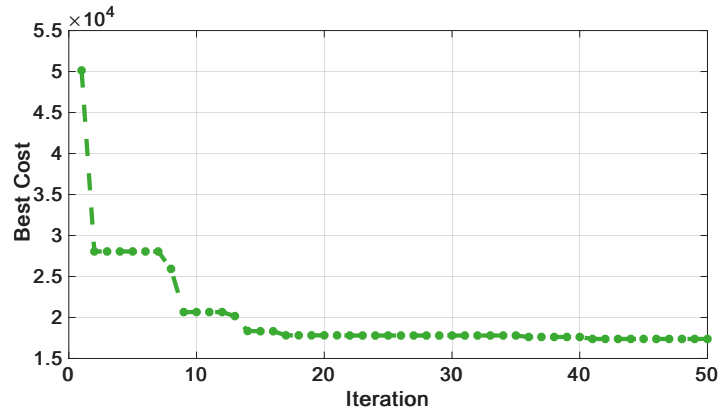


**Figure 6.** Convergence curve for four-parameter identification.

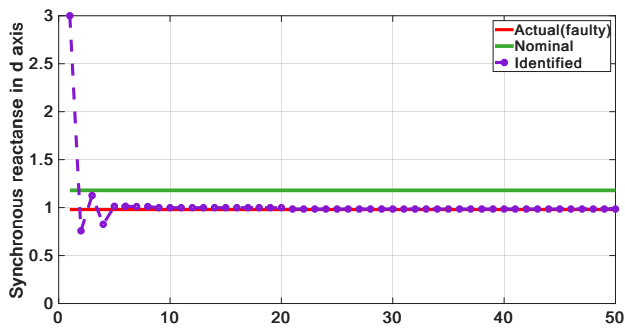
process. This indicates that when the health of the system is assured, identifying only the most sensitive parameters yields more precise results. The estimated values for  $X_d$  and  $X'_d$  as demonstrated in Table 6 are close to their actual faulty values, confirming the presence of the eccentricity fault.

**Table 6.** The results statement of scenario 2, case2.

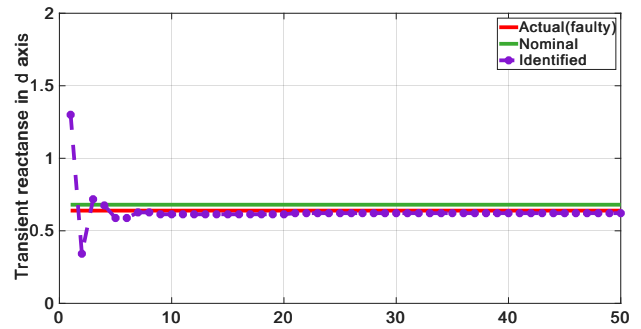
Parameter (p.u.)	Estimated Value (MPSO)	Nominal Value	Actual Value (Faulty)	Error (%)
$X_d$	0.9852	1.18	0.984	0.12
$X'_d$	0.6216	0.68	0.64	2.8

### 4.3. Scenario 3: Identification of $H$ , $X_d$ , $X'_d$

In this scenario, a 10% deviation in the inertia constant  $H$  is introduced alongside a 10% DE fault to assess the effectiveness and reliability of the proposed method. The parameters to be identified are  $H$ ,  $X_d$ , and  $X'_d$ . The goal is to demonstrate that, even with simultaneous deviations in  $H$  and the occurrence of a DE fault, the method remains capable of accurately identifying the faulty reactances  $X_d$  and  $X'_d$ , as well as the incorrect value of  $H$ .



(a) Identification of  $X_d$



(b) Identification of  $X'_d$

**Figure 7.** Parameter identification for  $X_d$  and  $X'_d$  for scenario 2, case 2.

The results in Table 7 show that significant deviations in  $X_d$  and  $X'_d$  are detected, signaling the presence of the DE fault, while the 10% deviation in  $H$  is also correctly identified. This scenario demonstrates the effectiveness of the method in handling multiple parameter deviations, ensuring the accurate detection of faults in complex operating conditions.

**Table 7.** The results statement of scenario 3.

Parameter (p.u.)	Estimated Value (MPSO)	Nominal Value	Actual(Faulty)Value	Error (%)
$H$	3.4994	3.2	3.52	0.58
$X_d$	0.9862	1.18	0.984	0.22
$X'_d$	0.6208	0.68	0.64	3

Even though the inertia constant  $H$  deviates by 10%, the method remains effective in detecting the DE fault through significant deviations in  $X_d$  and  $X'_d$ . Moreover, the incorrect  $H$  value is also correctly identified, highlighting the robustness of the approach in dealing with simultaneous parameter deviations. This scenario confirms the method's ability to diagnose both mechanical and electrical issues in generator systems with high accuracy.

#### 4.4. Scenario 4: Identification under 30% DE fault

To further validate the robustness of the proposed MPSO-based identification method, a 30% DE fault representing a severe mechanical deformation was simulated. This case introduces a pronounced distortion in the air-gap field, significantly affecting the machine's  $d$ -axis reactances. Using the same MPSO configuration as in previous tests, the method accurately captured the expected reduction in both  $X_d$  and  $X'_d$ , consistent with the finite element results. The estimated values closely matched the fault reference, as summarized in Table 8, confirming that the proposed algorithm maintains high accuracy even under severe fault conditions.

**Table 8.** Identification results under 30% DE fault.

Parameter (p.u.)	Estimated Value (MPSO)	Nominal	Actual (Faulty)	Error (%)
$X_d$	0.9529	1.180	0.950	0.3
$X'_d$	0.6350	0.680	0.633	0.3

## 5. Conclusion

This study presented a noninvasive and data-driven approach for early detection of DE faults in SPSCs using a hybrid framework that combines FEM with MPSO-based parameter identification. The method relies solely on measured three-phase current signals, avoiding the need for additional sensors or intrusive hardware modifications. By integrating FEM-derived fault signatures with the MPSO estimation process, the proposed approach effectively captures parameter deviations even for low-severity eccentricity levels, confirming its applicability for practical hydropower monitoring systems.

The simulation results under multiple fault scenarios demonstrated that the proposed algorithm can accurately track key machine parameters ( $X_d$ ,  $X'_d$ ,  $X_q$ , and  $H$ ) with minimal identification error. The approach maintained robustness under varying noise conditions and achieved convergence within one hour of computation, supporting its suitability for near-real-time diagnostic applications. Furthermore, the additional

30% DE fault case validated the method's stability under severe mechanical deformation, showing consistent agreement with finite element reference data. Overall, the study confirms that combining FEM-based insight with metaheuristic optimization offers a powerful framework for early, reliable, and nonintrusive fault detection in large synchronous generators.

## 6. Future work

Future developments will focus on enhancing the practicality and generalization of the proposed fault identification framework. First, real-time validation will be pursued by integrating the MPSO algorithm with monitoring platforms to process continuously acquired current data. This will help confirm its effectiveness under real operating conditions and different machine types. Second, higher sampling rates (up to 1 kHz) will be investigated to quantify the minimum data resolution required for stable identification without high computational cost. Finally, future work will include the experimental validation of fault cases using controlled test benches or digital twins to address the lack of real faulty-machine data and improve confidence in full-scale implementation.

## 7. Author contributions

Atena Tazikheh Lemeski: Writing—original draft, visualization, software, methodology, formal analysis.

Didem Tekgun: Writing—review & editing, validation, methodology, formal analysis, conceptualization.

Ozan Keysan: Writing—review & editing, supervision, conceptualization.

Kemal Leblebicioğlu: Writing—review & editing, supervision, and conceptualization.

Murat Göl: Writing—review & editing, validation, supervision, and conceptualization.

## References

- [1] Lipo TA. Analysis of synchronous machines, CRC press, 2017. <https://doi.org/10.1201/b12211>
- [2] Gyftakis KN, Platero CA, Zhang Y, Bernal S. Diagnosis of static eccentricity in 3-phase synchronous machines using a pseudo zero-sequence current, *Energies* 2019;12 (13):2476. <https://doi.org/10.3390/en12132476>
- [3] Ehya H, Faiz J. Electromagnetic analysis and condition monitoring of synchronous generators, 2022. <https://doi.org/10.1002/9781119636151>.
- [4] Reza Mortezaei S, Hosseini Aliabadi M, Javadi S. Eccentricity fault detection in surface-mounted permanent magnet synchronous motors by analytical prediction, fem evaluation, and experimental magnetic sensing of the stray flux density, *Journal of Magnetism and Magnetic Materials* 589 (2024) 171441. <https://doi.org/10.1016/j.jmmm.2023.171441>
- [5] Bruzzese C, Joksimovic G. Harmonic signatures of static eccentricities in the stator voltages and in the rotor current of no-load salient-pole synchronous generators, *IEEE Transactions on Industrial Electronics* 2010; 58 (5): 1606–1624. <https://doi.org/10.1109/TIE.2010.2087296>
- [6] Tekgun D. Influence of eccentricity faults on ipm motor equivalent circuit characteristics, in: 2025 7th Global Power, Energy and Communication Conference (GPECOM), IEEE, Bochum, Germany, 2025; 311–315. <https://doi.org/10.1109/GPECOM65896.2025.11061917>
- [7] Xu Q, Yuan S, Liu X, Pong PW, Liu C. Online detection and location of eccentricity fault in pmsg with external magnetic sensing, *IEEE Transactions on Industrial Electronics* 2022;69 (10): 9749–9760. <https://doi.org/10.1109/TIE.2022.3159947>
- [8] Bruzzese C. Diagnosis of eccentric rotor in synchronous machines by analysis of split-phase currents—part ii: Experimental analysis, *IEEE Transactions on Industrial Electronics* 2013;61 (8): 4206–4216. <https://doi.org/10.1109/TIE.2013.2284554>

- [9] Gong X, Qiao W. Current-based mechanical fault detection for direct-drive wind turbines via synchronous sampling and impulse detection, *IEEE Transactions on Industrial Electronics* 2014;62 (3): 1693–1702. <https://doi.org/10.1109/TIE.2014.2363440>
- [10] Sadeghi I, Ehya JH, Faiz, Analytic method for eccentricity fault diagnosis in salient-pole synchronous generators, in: 2017 International Conference on Optimization of Electrical and Electronic Equipment (OPTIM) ‘I&’ 2017 Intl Aegean Conference on Electrical Machines and Power Electronics (ACEMP), IEEE, 2017; 261–267. <https://doi.org/10.1109/OPTIM.2017.7974981>
- [11] Valavi M, Jørstad KG A, Nysveen, Electromagnetic analysis and electrical signature-based detection of rotor inter-turn faults in salient-pole synchronous machine, *IEEE Transactions on Magnetics* 2018;54 (9): 1–9. <https://doi.org/10.1109/TMAG.2018.2854670>
- [12] Bruzzese C, Giordani A, Santini E. Static and dynamic rotor eccentricity on-line detection and discrimination in synchronous generators by no-load emf space vector loci analysis, in: 2008 International Symposium on Power Electronics, Electrical Drives, Automation and Motion, IEEE, 2008: 1259–1264. <https://doi.org/10.1109/SPEEDHAM.2008.4581180>
- [13] Shaikh MF, Kim Hj, Lee SB, Lim C. Online airgap flux based diagnosis of rotor eccentricity and field winding turn insulation faults in synchronous generators, *IEEE Transactions on Energy Conversion* 2021; 37 (1): 359–366. <https://doi.org/10.1109/TEC.2021.3092198>
- [14] Gyftakis KN, Platero CA, Nøland JK. Multi-parametric condition monitoring of medium-power generators with brushless exciters under mechanical faults, *IEEE Transactions on Industry Applications*, 2023. <https://doi.org/10.1109/TIA.2023.3294902>
- [15] Ehya H, Nysveen A, Antonino-Daviu JA. Advanced fault detection of synchronous generators using stray magnetic field, *IEEE Transactions on Industrial Electronics* 2021;69 (11): 11675–11685. <https://doi.org/10.1109/TIE.2021.3118363>
- [16] Liao W, Wang T, Huang S. Fault diagnosis method of static inclined eccentricity of synchronous generator rotor based on FWA-RF, *Association for Computing Machinery*, New York, NY, USA, 2025, p. 404–409. <https://doi.org/10.1145/3729706.3729770>
- [17] Tabatabaei I, Faiz J, Lesani H, Nabavi-Razavi M. Modeling and simulation of a salient-pole synchronous generator with dynamic eccentricity using modified winding function theory, *IEEE Transactions on Magnetics* 2004; 40 (3): 1550–1555. <https://doi.org/10.1109/TMAG.2004.826611>
- [18] Faiz J, Tabatabaei I. Extension of winding function theory for nonuniform air gap in electric machinery, *IEEE Transactions on Magnetics* 2002; 38 (6): 3654–3657. <https://doi.org/10.1109/TMAG.2002.804805>
- [19] Mostafaei M, Faiz J. An overview of various faults detection methods in synchronous generators, *IET electric power applications* 2021;15 (4):391–404. <https://doi.org/10.1049/elp2.12031>
- [20] Mirimani SM, Vahedi A, Marignetti F, Di Stefano R. An online method for static eccentricity fault detection in axial flux machines, *IEEE Transactions on Industrial Electronics* 2014;62 (3): 1931–1942. <https://doi.org/10.1109/TIE.2014.2360070>
- [21] Ehya H, Nysveen A, Akin B, Gyftakis KN. An expeditious algorithm for identification and classification of rotor faults in salient pole synchronous generators, *IEEE Transactions on Industrial Electronics* 2023; 71 (2): 2008–2017. <https://doi.org/10.1109/TIE.2023.3253954>
- [22] Ehya H, Nysveen A, Nilssen R, Liu Y. Static and dynamic eccentricity fault diagnosis of large salient pole synchronous generators by means of external magnetic field, *IET Electric Power Applications* 2021; 15 (7): 890–902. <https://doi.org/10.1049/elp2.12068>
- [23] Liu Z, Zhang P, He S, Huang J. A review of modeling and diagnostic techniques for eccentricity fault in electric machines, *Energies* 2021; 14 (14): 4296. <https://doi.org/10.3390/en14144296>

- [24] Lemeski AT, Ebrahimi R, Zakariazadeh A. Optimal decentralized coordinated operation of electric vehicle aggregators enabling vehicle to grid option using distributed algorithm, *Journal of Energy Storage* 2022; 54: 105213. <https://doi.org/10.1016/j.est.2022.105213>
- [25] Tazikeh Lemeski A, Ebrahimi R, Zakariazadeh A, Firuzi K. Energy and reserve scheduling of distribution network in presence of electric vehicle aggregators: A decentralized approach, *International Transactions on Electrical Energy Systems* 2025 (1): 2291677. <https://doi.org/10.1155/etep/2291677>
- [26] Mafruddin MM, Suwarno S, Abu-Siada A. Finite element simulation of a 126 mw salient pole synchronous generator with rotor eccentricity, in: 2019 2nd International Conference on High Voltage Engineering and Power Systems (ICHVEPS), IEEE, 2019, 1–96. <https://doi.org/10.1109/ICHVEPS47643.2019.9011072>
- [27] Acilan E, Gol M. Novel parameter error identification method for power plant dynamic models, *IEEE Transactions on Power Systems* 2023;39 (1):957–966. <https://doi.org/10.1109/TPWRS.2023.3253842>
- [28] Lee D. Ieee recommended practice for excitation system models for power system stability studies (ieee std 421.5-1992), Energy Development and Power Generating Committee of the Power Engineering Society 1992; 95 (96). <https://doi.org/10.1109/IEEESTD.1992.106975>
- [29] Mover WGP, Supply E. Hydraulic turbine and turbine control models for system dynamic studies, *IEEE Transactions on Power Systems* 1992;7 (1): 167–179. <https://doi.org/10.1109/59.141700>